

Strain analysis in SiN/Ge microstructures obtained via Si-complementary metal oxide semiconductor compatible approach

G. Capellini, G. Kozlowski, Y. Yamamoto, M. Lisker, C. Wenger et al.

Citation: *J. Appl. Phys.* **113**, 013513 (2013); doi: 10.1063/1.4772781

View online: <http://dx.doi.org/10.1063/1.4772781>

View Table of Contents: <http://jap.aip.org/resource/1/JAPIAU/v113/i1>

Published by the [American Institute of Physics](#).

Related Articles

A grillage model for predicting wrinkles in annular graphene under circular shearing

J. Appl. Phys. **113**, 014902 (2013)

Effect of alloying element Al substitution on Ni-Mn-Sn shape memory alloy by first-principle calculations

J. Appl. Phys. **112**, 123723 (2012)

Dynamic behavior of acrylic acid clusters as quasi-mobile nodes in a model of hydrogel network

J. Chem. Phys. **137**, 244908 (2012)

Cyclic impulsive compression loading along the radial and tangential wood directions causes localized fatigue

J. Appl. Phys. **112**, 124913 (2012)

On the elastic, elastic-plastic properties of Au nanowires in the range of diameter 1-200nm

J. Appl. Phys. **112**, 123522 (2012)

Additional information on J. Appl. Phys.

Journal Homepage: <http://jap.aip.org/>

Journal Information: http://jap.aip.org/about/about_the_journal

Top downloads: http://jap.aip.org/features/most_downloaded

Information for Authors: <http://jap.aip.org/authors>

ADVERTISEMENT



AIP Advances

Now Indexed in
Thomson Reuters
Databases

Explore AIP's open access journal:

- Rapid publication
- Article-level metrics
- Post-publication rating and commenting

Strain analysis in SiN/Ge microstructures obtained via Si-complementary metal oxide semiconductor compatible approach

G. Capellini,^{1,2,a)} G. Kozłowski,² Y. Yamamoto,² M. Lisker,² C. Wenger,² G. Niu,² P. Zaumseil,² B. Tillack,^{2,3} A. Ghrib,⁴ M. de Kersauson,⁴ M. El Kurdi,⁴ P. Boucaud,⁴ and T. Schroeder^{2,5}

¹*Dipartimento di Fisica “E. Amaldi”, Università degli Studi Roma Tre, via Vasca Navale 84, 00146 Roma, Italy*

²*IHP, Im Technologiepark 25, 15236 Frankfurt (Oder), Germany*

³*Technische Universität Berlin, HFT4, Einsteinufer 25, 10587 Berlin, Germany*

⁴*Institut d’Electronique Fondamentale, CNRS-Université Paris-Sud F-91405 Orsay, France*

⁵*Brandenburgische Technische Universität, Konrad-Zuse-Strasse 1, 03046 Cottbus, Germany*

(Received 28 September 2012; accepted 5 December 2012; published online 4 January 2013)

We have analyzed the strain distribution and the photoluminescence in Ge microstructures fabricated by means of a Si-CMOS compatible method. The tensile strain in the Ge microstructures is obtained by using a SiN stressor layer. Different shapes of microstructure, allowing the Ge layers to freely expand into one, two, or three dimensions, resulted in different strain distribution profiles. Maximal equivalent biaxial tensile strain values up to $\sim 0.8\%$ have been measured. Room temperature photoluminescence emission has been observed and attributed to direct-band gap recombination spectrally shifted by tensile strain. © 2013 American Institute of Physics.

[<http://dx.doi.org/10.1063/1.4772781>]

INTRODUCTION

Over the last decade, rapid advances in Si photonics have enabled the mass production of higher functionality and lower cost photonic components (such as waveguides, modulators, and photodetectors) integrated with electronic circuitry in silicon complementary metal oxide semiconductor technology (Si-CMOS).¹ The major outstanding hurdle to realize a low-cost, fully functional silicon-photonic platform is the realization of a monolithically integrated laser.² The integration of the light source would lead to cost reduction, increased yield, easing of the packaging, and link-budget improvement. Among several proposed integration approaches, integrated lasers comprising active regions based on III-V/Si or SiGe/Si heterostructures are especially interesting.² In particular, Ge/Si heteroepitaxial layers are very promising since Ge is now considered a “fab”-compatible material¹ and is deemed as one of the most promising material for “more than Moore” device development.³

Both optically⁴ and electrically⁵ pumped Ge-on-Si lasers have already been demonstrated. To achieve this goal, the authors exploited the residual tensile strain, of the order of $\varepsilon = 0.2\%$, accumulated during the growth process⁶ and n -type doping into the Ge layer. The tensile strain induces a shift of the Γ and L valleys of the Ge conduction band which results in a decrease of their energy difference and a consequent higher percentage of electrons in the higher energy Γ valley. If population inversion is achieved, a direct bandgap optical gain can be observed.⁷ The excess carrier density needed to realize this condition is high ($\sim 10^{20} \text{ cm}^{-3}$). Such high density generates parasitic absorption, limiting the net optical gain. Although optical gain values as high as

1000 cm^{-1} are expected in highly phosphorous-doped Ge layers ($\sim 10^{20} \text{ cm}^{-3}$), a maximum gain of $\sim 50 \text{ cm}^{-1}$ has been reported.⁷ This remarkable difference can be due to the inherent difficulty to achieve the requested high active n -type doping density in Ge,⁸ and/or, as recently suggested in Ref. 9, to an oversimplification of the optical gain model proposed in Refs. 4 and 5 which does not include valence intraband absorption. As a consequence, a rather high threshold current density for lasing has been reported ($\sim 10^5 \text{ A.cm}^{-2}$) that limits the emitted optical power due to contact breakdown.

If the Γ - L energy barrier is decreased by applying higher tensile strain, much lower densities of injected carriers are needed and higher net optical gain values can be achieved. A tensile strain value of $\varepsilon \sim 2\%$ is enough to induce a Γ - L cross-over leading toward a “direct-type” gap structure in Ge.¹⁰ Upon using tensile strain in the 2-3% range, net optical gain value of $\sim 3000 \text{ cm}^{-1}$ value are expected for n -type doping density of $8 \times 10^{18} \text{ cm}^{-3}$, an easier-to-achieve donor density. Moreover, for doping density below 10^{19} cm^{-3} , the gain is expected to increase with the operating temperature with a maximum at 350 K, a value close to typical on-chip temperatures.¹⁰ Therefore, different fabrication approaches based on micromechanical engineering¹⁰⁻¹² or on the use of stressor layers¹³⁻¹⁶ have been proposed to achieve tensile strained Ge microstructures suitable for optoelectronic applications.

The applied mechanical stress results in a strain distribution dependent on the Ge structure shape and on its capability to elastically relax by lateral expansion and/or bending. This inhomogeneous strain distribution is expected to influence the optical properties of the Ge microstructures. In particular, it would be highly desirable to understand its effect on the gain mechanism in tensile Ge.⁹

In this paper, we investigate the strain distribution and the photoluminescence (PL) in Ge microstructures fabricated on Silicon-on-insulator (SOI) substrate by means of a Si-CMOS

^{a)}Author to whom correspondence should be addressed. Electronic mail: capellini@fis.uniroma3.it.

compatible method. The tensile strain in the Ge microstructures is obtained by using a compressively strained SiN stressor layer. Microstructures of different types have been fabricated, allowing the Ge layers to freely expand into one, two, or three dimensions, resulting in different strain distribution profiles along the structure as probed by micro-Raman spectroscopy. Maximal tensile strain values up to $\varepsilon \sim 0.8\%$ have been measured. Room temperature PL emission has been observed and attributed to direct-band gap recombination upon comparison with 30 band **k.p** calculations.

EXPERIMENTAL AND FABRICATION METHOD

The investigated microstructures were fabricated in the state-of-the-art $0.13 \mu\text{m}$ BiCMOS process line at IHP on $8''$ SOI wafers.

First, we deposited a 400 nm-thick Ge layer by reduced pressure chemical vapor deposition (RPCVD) using a two-temperature process comprising the deposition at $T = 300^\circ\text{C}$ of a Ge seed layer followed by a high temperature growth step at 550°C . Several cycles of annealing at 800°C have been performed during the Ge deposition to reduce threading dislocation density as detailed in Ref. 17. On top of the Ge layer, a 400 nm-thick SiN stressor layer was deposited on top of Ge by plasma enhanced chemical vapor deposition (PECVD) using a mixture of SiH_4 and NH_3 using N_2 as carrier gas. The SiN layer deposition conditions were selected to maximize the residual *compressive* stress in the stressor layer. After the deposition of the stressor layer, another SiN layer was deposited on the wafer back to prevent wafer bowing and, consequently, to avoid chucking issues during the fabrication process. The micro-structures were then fabricated out of the deposited SiN/Ge/SOI stack using a standard lithographic process.

Selected areas of the stack were removed by reactive ion etching, exposing the underlying buried oxide layer (BOX). In such a way, micro-strips of Ge attached to the substrate were fabricated. The length l ranged between 10 and $60 \mu\text{m}$ (along the x -axis) and the width w between 1 and $10 \mu\text{m}$ (y) (Fig. 1(a)).

The second type of structures considered, i.e., the SiN/Ge/Si suspended micro-bridges shown in Fig. 1(b), was obtained upon removal of the $2 \mu\text{m}$ -thick BOX using a 5% HF buffered wet-etch solution.

Selected micro-bridges were then detached from the surrounding blanket material using a focused ion beam (FIB) in order to allow the structures to freely expand in all the three dimensions Fig. 1(c). We point out that FIB was only used to save development time and the cost of a mask-set, but the same process can be performed using standard clean room lithographic processes.

Micro-Raman measurements were performed after each fabrication step in order to evaluate the elastic strain into the realized micro-structures. We have used an InVia Renishaw spectrometer working in backscattering geometry equipped with a 633-nm laser focused to a spot of $\sim 0.8 \mu\text{m}$ in diameter using a $100\times$ objective lens with a numerical aperture of 0.85. The laser penetration depth in the Ge layer is $\sim 90 \text{ nm}$. The laser power was low enough to prevent heating of the material, as proved by monitoring the peak position of the Raman Ge-Ge mode over a long acquisition time. Each micro-structure was characterized by a series of measurements in its half and at a quarter of its length. Additional measurements were performed on the blanket stack 10 and $20 \mu\text{m}$ away from the structure's edge. The Raman shift of Ge-Ge mode $\omega_{\text{Ge-Ge}}$ in micro-structures was measured with respect to the Ge-Ge phonon mode energy as measured in a Ge(001) reference bulk crystal ($\omega_{\text{Ge-Ge}}^0 = 300.17 \text{ cm}^{-1}$). The equivalent in-plane biaxial strain $\varepsilon^{\text{bi}} = \varepsilon_x = \varepsilon_y$ was calculated using the relationship¹⁸

$$\frac{\omega_{\text{Ge-Ge}} - \omega_{\text{Ge-Ge}}^0}{-390} = \varepsilon^{\text{bi}} \quad (1)$$

This relationship was obtained measuring by means of X-ray diffraction the biaxial strain in Ge/Si unstructured layers of different thickness and thus at different stages of their plastic relaxation. Strain values between -1.5% and -0.12% were obtained in Ge/Si layers having a thickness ranging in the 5-50 nm range. The measurements were performed with a SmartLab diffractometer from Rigaku equipped with a 9 kW rotating anode Cu source, a Ge(400) $\times 2$ crystal collimator, and a Ge(220) $\times 2$ crystal analyzer. The Bragg peak positions of Ge(004) and asymmetric (224) reflections were used to measure the in plane and out of plane lattice parameters. Raman shifts were then measured in 30 points of each Ge/Si blanket wafers to increase statistical accuracy. The measured strain-shift coefficient is $b = -390 \pm 25 \text{ cm}^{-1}$, in very good agreement with the values reported in literature.¹⁸

Numerical simulations of the strain field distribution were carried out using the Flex-PDE commercial package based on the finite element method (FEM).¹⁹ Photoluminescence (PL) measurements were performed at room temperature (RT) using a 532 nm excitation wavelength and a micro-PL set-up, comprising a 50 cm spectrometer and an extended InGaAs photodetector. Also in this case, a low excitation power was used to prevent heating of the micro-structures.

We emphasize that for the majority of processed micro-structures, the strain is not purely biaxial, as evidenced by finite element simulations. We did however use the notion of an equivalent biaxial strain deduced from

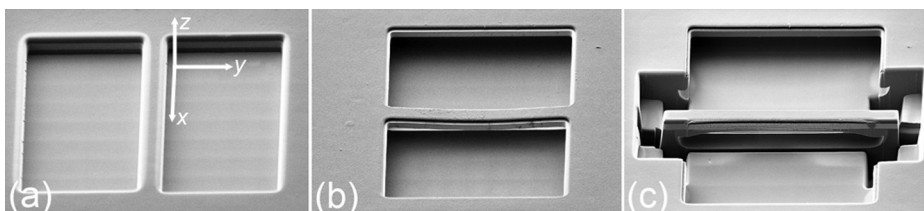


FIG. 1. Scanning electron microscope (SEM) image of typical micro-structure ($l = 20 \mu\text{m}$, $w = 2 \mu\text{m}$) at three different fabrication steps: (a) micro-stripe definition upon window opening in to the SiN/Ge/SOI stack, (b) under-etching, and (c) after final trimming and detachment.

Raman measurements following Eq. (1) to quantitatively compare different structures. The equivalent biaxial strain is indeed a relevant parameter to describe the effect of strain on the electronic band structure and the degree of carrier injection needed to achieve population inversion.

RESULTS AND DISCUSSIONS

First, we focus on blanket, unstructured SiN/Ge/SOI stack. By optimizing the stressor deposition parameters, a high compressive stress of $\sigma_{SiN} = -2$ GPa in the SiN layer on Ge/SOI was obtained, as calculated by measuring the wafer curvature and using the Stoney equation.²⁰ Raman measurements performed on a blanket SiN/Ge/SOI wafer (not shown) indicate a tensile strain value in Ge of $\varepsilon = 0.26\%$, a value very close to that measured on Ge/SOI layer which is due to the different coefficient of thermal expansion in Ge and Si.⁶ Therefore, the stressor layer does not significantly affect the strain in un-patterned Ge layer.

In Fig. 2(a), we report the measured Raman shift and the value of the corresponding equivalent biaxial strain for the micro-structured Ge layers of Fig. 1 ($l = 20 \mu\text{m}$, $w = 2 \mu\text{m}$, square) after each of the three process steps: (i) defining a micro-stripe (blue markers); (ii) under-etching and releasing the micro-bridge from the substrate (red); (iii) trimming the micro-bridge (green). Data for micro-structures having same length and $w = 1 \mu\text{m}$ (circle) are reported also for comparison and will be discussed in the following.

Immediately after the first stage of the micro-stripe patterning, the tensile strain in Ge is increased, reaching a maximal value of $\varepsilon \sim 0.5\%$ in the middle of the structure. Thus, the tensile strain value nearly doubles with respect to the unpatterned Ge layer, even though the structures are firmly attached to the underlying BOX.

In order to analyze the SiN relaxation mechanism and the resulting accumulation of tensile strain in the Ge layer, we now discuss the displacement field as calculated by FEM in a cross section at the center ($x = 0$; yz plane, Fig. 2(b)) of a $l = 20 \mu\text{m}$ long and $w = 2 \mu\text{m}$ wide micro-stripe, i.e., the micro-structure shown in Fig. 1(a). Only displacement field components tangential to the displayed planes are shown.

The displacement field into the SiN layer is due to the relaxation of the initial compressive stress which occurs mostly along the y direction. This relaxation “pulls” the Ge layer and induces the accumulation of tensile strain. The displacement field is not homogeneous in the structure. In particular, the displacement along the micro-stripe axis x is hindered by the surrounding blanket material, whereas the relaxation along the z direction, normal to the substrate, is prevented by the underlying attached BOX as shown in Fig. 2(b). In consequence, the stress originating from the SiN layer is partially released at free surfaces along the edges of the micro-stripe towards the trenches opened in the stack. This result demonstrates that the strain field is not purely biaxial and that the total strain is dominated by the displacement along the y direction.

A more detailed analysis of the strain distribution along the x -axis is reported in Fig. 2(c), where we show the comparison between Raman measured biaxial strain (square) and

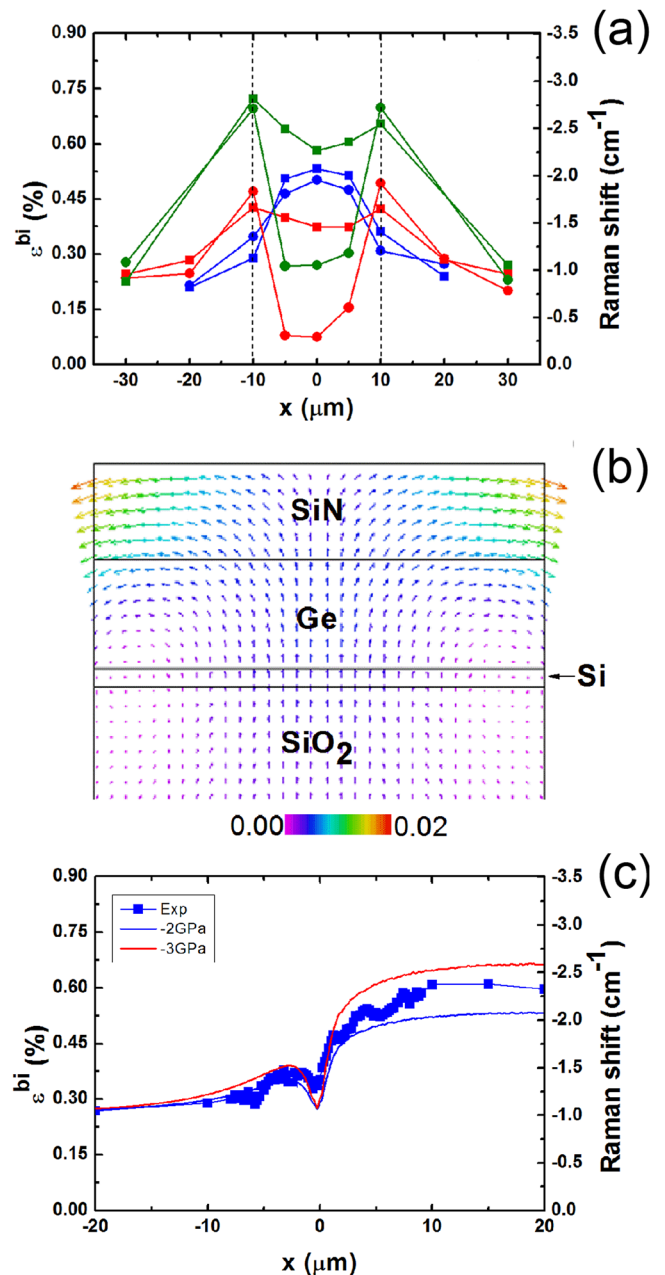


FIG. 2. (a) Biaxial strain values (left axis) and measured Raman shift measured along the x -axis of two Ge microstructures ($l = 20 \mu\text{m}$, center at $x = 0$) having width of $1 \mu\text{m}$ (circle) and $w = 2 \mu\text{m}$ (square), after: defining a micro-stripe (blue markers), under-etching and releasing the micro-bridge from the substrate (red), and trimming the micro-bridge (green). The vertical dotted lines define the micro-structure length. (b) Displacement field calculated for a $l = 20 \mu\text{m}$ long and $w = 2 \mu\text{m}$ wide micro-stripe at its center (yz plane cross section at $x = 0$). (c) Biaxial strain and measured Raman shift as measured (square) or calculated ($\sigma_{SiN} = -2$ GPa blue line, $\sigma_{SiN} = -3$ GPa red line) in half microstripe $l = 40 \mu\text{m}$ long and $w = 2 \mu\text{m}$ wide. The origin $x = 0$ is set at the end of the edge of the microstripe, negative values correspond to measurements on the unpatterned region of the surface.

the results obtained from FEM simulations (lines) for a micro-stripe having $l = 40 \mu\text{m}$ and $w = 2 \mu\text{m}$. For symmetry reason, we have plotted only half of the structure. The origin is set at one of the ends of the patterned microstripe. The biaxial strain away from the structure is exactly the same as the one measured in the unpatterned wafer. The equivalent tensile strain is observed to increase already $5 \mu\text{m}$ away from

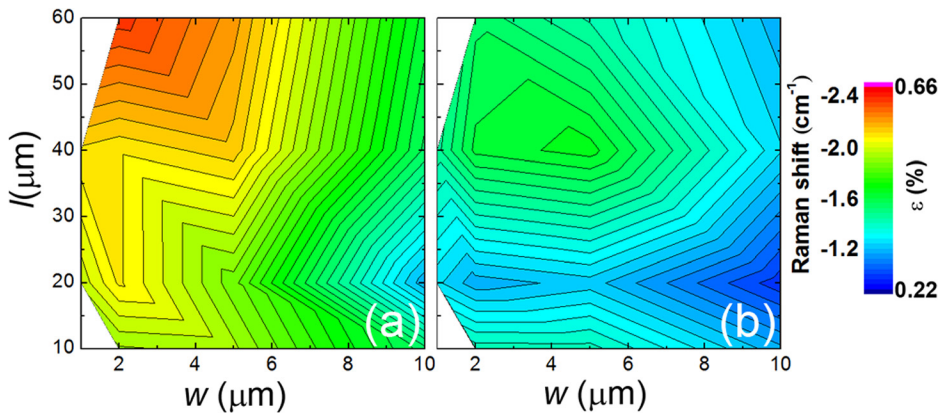


FIG. 3. Raman shift and biaxial strain values in Ge at the center (a) and at the junction with the blanket stack (b) for different lengths l and widths w of a micro-stripe.

the microstripe end and it monotonically increases into the patterned structure and reaches a plateau at about one fourth of the stripe length. The FEM simulation reproduces very well the observed behavior along the structure, including the presence of a dip at the very edge of the microstripe due to uniaxial compression of the Ge layer along the y and z directions. The initial SiN compressive stress value was set to be in the $(-2; -3)$ GPa range: the good agreement with the measured data confirms that the blanket SiN/Ge stack relaxed only where the microstructures were fabricated.

In Fig. 3, we report the Raman shift together with the biaxial strain value in Ge measured (a) at the center and (b) at the junction with the blanket stack for different lengths and widths of a micro-stripe. The strain measured at the center increases for narrower and longer stripes and is larger than the tensile strain at the junction with the blanket stack. The maximum observed strain amounts to $\sim 0.6\%$ for stripes having $l = 60 \mu\text{m}$ and $w = 2 \mu\text{m}$. A similar behavior is observed for the strain measured at the edge of the micro-stripes, although the strain variation with size is less intense. In order to maximize the strain field in germanium microstripes, it is thus preferable to select structures with large lengths and small widths.

The subsequent fabrication step comprised the detachment of the micro-stripes from the substrate upon etching the BOX underneath (see Fig. 1(b)). As a result, the stress accumulated in the SiN-stressor is partially released by bending of the suspended micro-bridge. FEM simulations in Fig. 4 show that the bending is caused by the force exerted on the detached bridge by the surrounding wafer regions. In Fig. 4(a), the under-etched edge of the blanket stack is observed to bend downwards (see arrows) and to exert a force on the micro-bridge. This phenomenon is highlighted by the displacement field reported in plan-view and cross-section in Figs. 4(b) and 4(c), respectively. Although the micro-bridge

itself counteracts this force, the resulting force induces a downward bending. This entails a compression of the middle section and tension of the micro-bridge edges, in agreement with the Raman measurements reported in Fig. 2(a). Although still tensile, the strain in the center ($0.1\text{--}0.4\%$) is evidently smaller than the strain at the edge of the micro-structure ($0.4\text{--}0.45\%$). The comparison of two presented widths indicates (see Fig. 2(a)), that wider bridges counteract more efficiently the external force and are characterized by more homogeneous strain field. On the contrary, narrower bridges have a high gradient of strain along the micro-bridge axis. Interestingly, *compressive* strain was observed in the middle of very short and narrow micro-bridges (not shown).

Finally, micro-bridges edges were detached from the surrounding blanket stack as shown in Fig. 1(c). These trimmed micro-bridges bent upwards. The external force acting from the surrounding blanket is removed and the stress stored in the SiN layer can be completely relaxed. A closer look on the strain values reported in Fig. 2(a) indicates that the trimming induces, as compared to the released micro-bridge, an increase of tensile strain in the whole structure by roughly 0.25% with a maximum values at its edges.

In Fig. 5, we present the comparison between the strain values measured at the edge of underetched and trimmed micro-bridges having the same width $w = 2 \mu\text{m}$ and length l in the $10\text{--}60 \mu\text{m}$ range. We can observe that the structure length has a larger impact on the strain in underetched micro-bridges than in their trimmed counterparts ($\sim 0.11\%$ and $\sim 0.06\%$ variation in the investigated range). A maximum tensile strain value of $\varepsilon = 0.8\%$ was measured in the longest trimmed micro-bridge here investigated. This value is very similar to the maximum value obtained in Ref. 15, although we achieved it in a structure having a wafer footprint two order of magnitude smaller. We point here out that the tensile strain is

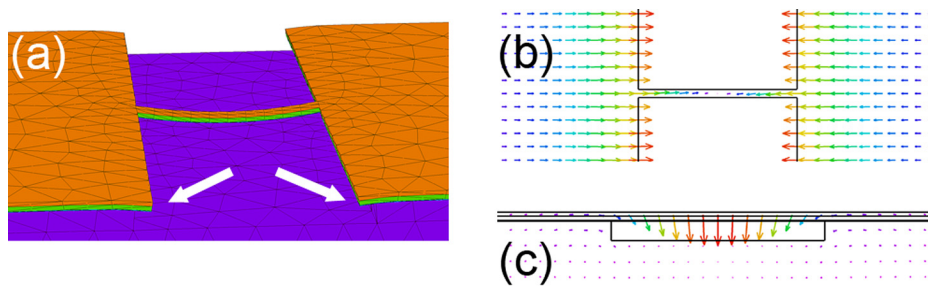


FIG. 4. Results of FEM simulation on micro-stripes detached from the substrate: (a) three dimensional results showing the downward bending of the structure, (b) plane view, and (c) cross section image of the calculated displacement field.

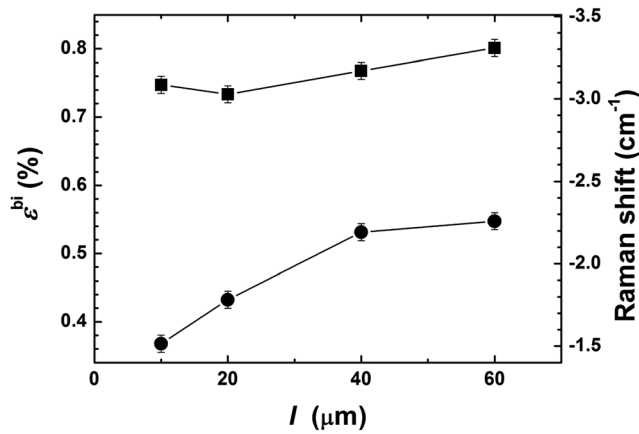


FIG. 5. Biaxial strain values and measured Raman shift, at the edge of under-etched (dot) and trimmed (square) $w = 2 \mu\text{m}$ wide micro-bridges as a function of the length l .

larger than 0.65% along the whole microbridge for the $2 \mu\text{m}$ large bridge. It indicates that this method is very efficient to induce large strains in structures with size compatible with optical waveguiding. We can observe that the maximum stress transfer is achieved in the case of trimmed structures which are however expected to have a smaller efficiency for heat dissipation. There is thus a trade-off between thermal budget management and maximum achievable tensile strain. Even if the strain amplitude is smaller for microstripes as shown in Fig. 2(a), these structures might be more suitable under high optical pumping necessary to achieve population inversion.

We next discuss the results of PL measurements. Figure 6 shows the RT-PL spectra of: (a) a micro-stripe measured at the center (top) and at its edge (bottom) and (b) a trimmed micro-bridge measured close to the edge. In both cases, the PL signal is dominated by a single peak convoluted with Fabry-Perot resonances which are correlated with the width of the structure. There is a clear red-shift of the PL peaks respect to the one observed in a reference blanket Ge wafer (PL peak at 1560 nm). The photoluminescence resonance can be compared with the one predicted by the modeling based on a 30

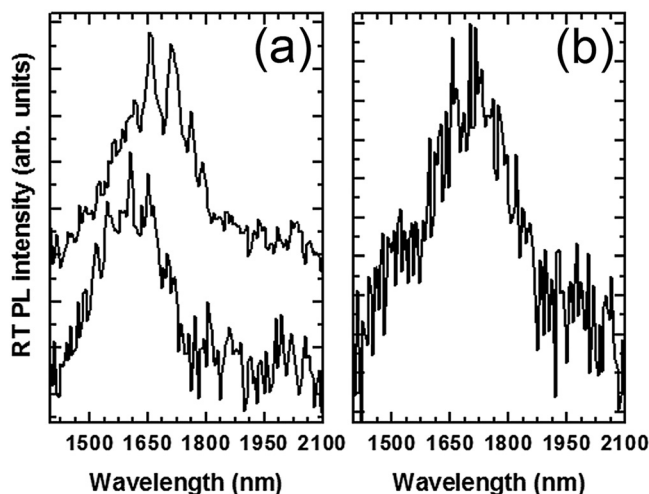


FIG. 6. (a) RT PL of a micro-stripe ($l = 60 \mu\text{m}$, $w = 5$) measured at its center (top) and at the structure edge (bottom). The curves have been offset for clarity. (b) Photoluminescence of a trimmed micro-bridge ($l = 40 \mu\text{m}$, $w = 2$) measured close to the edge.

band \mathbf{k}, \mathbf{p} description of the band structure which takes in to account the strain distribution simulated by FEM.²¹ From the modeling, we obtain that the peak resonance is sensitive to the photo-induced carrier density. At low excitation density, such the one here used, recombination associated with light-hole and heavy-hole bands contribute to the spectrum with similar amplitudes: we thus attribute the observed PL features to these recombination processes. As expected, the PL peak shifts toward longer wavelength for higher values of the tensile strain. The uncertainty in the determination of the exact position of the PL peaks is due to the broadening of the recombination, the Fabry-Perot resonances and the residual noise (low excitation power).

For the micro-stripe (Fig. 6(a)), the maximum is observed at a wavelength of 1615 nm at the edge of the structure and 1650 nm at the center, respectively. The tensile strain is thus observed to be significantly larger at the center of the stripe than at its edge, in agreement with Raman measurements reported in Fig. 2(a). In the case of the trimmed micro-bridge, the maximum photoluminescence intensity is observed at ~ 1700 nm. This confirms that the tensile strain at the edge of the trimmed micro-bridge is larger than the tensile strain at the edge of the under-etched structure, as seen in Fig. 2(a).

For the micro-stripe (center - Fig. 2(a)), the PL spectrum is consistent with a 0.6% equivalent biaxial strain in agreement with Raman measurement and with FEM modeling (we obtained by FEM modeling $\epsilon_y = 1.11\%$, $\epsilon_x = -0.12\%$, equivalent to a biaxial strain value $\epsilon^{bi} = 0.57\%$). For the trimmed structure, the PL spectrum is consistent with a 0.7% equivalent biaxial strain in agreement with strain values reported in Fig. 5 (0.76%). We note that the area probed by PL might differ from the one probed by Raman, therefore explaining the slight variations between different type of measurements.

CONCLUSIONS

In summary, we have discussed a fully Si-CMOS compatible approach to fabricate SiN/Ge/Si micro-structures comprising tensile strained Ge active layers. We have shown that by adjusting micro-structure size and shape, the strain distribution within Ge layer can be optimized and accurately controlled. Tensile strain values as large as $\sim 0.8\%$ were achieved. Room temperature direct band gap recombination was observed on these structures. The PL resonances have been found to depend on the microstructure strain distribution as measured by Raman scattering.

We believe that the SiN-stressor-based approach to tensile strained Ge will have high impact on the fabrication of integrated devices for photonic applications. Our future activities will aim at further increasing the tensile strain into the microstructure and optimizing the strain distribution within the Ge layer upon acting on the SiN-stressor deposition parameters and the micro-bridge geometry and orientation, with a design compatible with the realization of an optical cavity.

¹G. Masini, S. Sahni, G. Capellini, J. Witzens, and C. Gunn, *Adv. Opt. Technol.* **2008**, 196572 (2008).

²D. Lang and J. E. Bowers, *Nature Photon.* **4**, 511 (2010).

- ³See <http://www.itrs.net/> for “International Technology Roadmap for Semiconductors 2011.”
- ⁴J. Liu, X. Sun, R. Camacho-Aguilera, L. C. Kimerling, and J. Michel, *Opt. Lett.* **35**, 679 (2010).
- ⁵R. E. Camacho-Aguilera, Y. Cai, N. Patel, J. T. Bessette, M. Romagnoli, L. C. Kimerling, and J. Michel, *Opt. Express* **20**, 11316 (2012).
- ⁶G. Capellini, M. De Seta, P. Zaumseil, G. Kozłowski, and T. Schroeder, *J. Appl. Phys.* **111**, 073518 (2012).
- ⁷X. Sun, J. Liu, L. C. Kimerling, and J. Michel, *IEEE J. Sel. Top. Quantum Electron.* **16**, 124 (2010).
- ⁸H. Gamble, B. M. Armstrong, P. T. Baine, Y. H. Low, P. V. Rainey, S. J. N. Mitchell, and D. W. McNeill, in *Germanium Processing*, edited by A. Nazarov, J. P. Colinge, and F. Balestra (Springer, Berlin, Heidelberg).
- ⁹L. Carroll, P. Friedli, S. Neuenschwander, H. Sigg, S. Cecchi, F. Isa, D. Chrastina, G. Isella, Y. Fedoryshyn, and J. Faist, *Phys. Rev. Lett.* **109**, 057402 (2012).
- ¹⁰P. H. Lim, S. Park, Y. Ishikawa, and K. Wada, *Opt. Express* **17**, 16358 (2009).
- ¹¹D. Nam, D. Sukhdeo, A. Roy, K. Balram, S.-L. Cheng, K. C.-Y. Huang, Z. Yuan, M. Brongersma, Y. Nishi, D. Miller, and K. Saraswat, *Opt. Express* **27**, 25866 (2011).
- ¹²J. R. Sánchez-Pérez, C. Boztug, F. Chen, F. F. Sudradjat, D. M. Paskiewicz, R. B. Jacobson, M. G. Lagally, and R. Paiella, *Proc. Natl. Acad. Sci. U.S.A.* **108**, 18893 (2011).
- ¹³M. El Kurdi, H. Bertin, E. Martincic, M. de Kersauson, G. Fishman, S. Sauvage, A. Bosseboeuf, and P. Boucaud, *Appl. Phys. Lett.* **96**, 041909 (2010).
- ¹⁴M. de Kersauson, M. El Kurdi, S. David, X. Checoury, G. Fishman, S. Sauvage, R. Jakomin, G. Beaudoin, I. Sagnes, and P. Boucaud, *Opt. Express* **19**, 17925 (2011).
- ¹⁵J. R. Jain, A. Hryciw, T. M. Baer, D. A. B. Miller, M. L. Brongersma, and R. T. Howe, *Nature Photon.* **6**, 398 (2012).
- ¹⁶A. Ghrib, M. de Kersauson, M. El Kurdi, R. Jakomin, G. Beaudoin, S. Sauvage, G. Fishman, I. Sagnes, and P. Boucaud, *Appl. Phys. Lett.* **100**, 201104 (2012).
- ¹⁷Y. Yamamoto, P. Zaumseil, T. Arguirov, M. Kittler, and B. Tillack, *Solid-State Electron.* **60**, 2 (2011).
- ¹⁸T. S. Perova, J. Wasyluk, K. Lyutovic, E. Kasper, M. Oehme, K. Rode, and A. Waldron, *J. Appl. Phys.* **109**, 033502 (2011).
- ¹⁹See <http://www.pdesolutions.com/> for “FlexPDE, PDE Solutions Inc.”
- ²⁰G. G. Stoney, *Proc. R. Soc. London A* **82**, 172 (1909).
- ²¹M. El Kurdi, S. Sauvage, G. Fishman, and P. Boucaud, *J. Appl. Phys.* **107**, 013710 (2010).